Folding intermediates of SNARE complex assembly

Klaus M. Fiebig, Luke M. Rice, Elizabeth Pollock[1] and Axel T. Brunger

The Howard Hughes Medical Institute, Department of Molecular Biophysics and Biochemistry, and [1]Department of Chemistry, Yale University, New Haven, Connecticut 06520, USA.

SNARE (soluble NSF attachment protein receptor) proteins assemble into a stable complex essential for vesicle–membrane fusion. To further understand SNARE function we have used solution nuclear magnetic resonance (NMR) spectroscopy to characterize three assembly states of a yeast SNARE complex: first, the 'closed' conformation of Sso1; second, the binary complex of Sso1 and Sec9; and third, the ternary complex of Sso1, Sec9 and Snc1. Sec9 and Snc1 are unstructured in isolation. Sso1 likely consists of a four helix bundle formed by part of the C-terminal H_{core} domain and the N-terminal $H_AH_BH_C$ domain, and this bundle is flanked on both sides by large flexible regions. Sso1 switches to an 'open' state when its H_{core} domain binds Sec9. Conformational switching of the H_{core} domain, via $H_AH_BH_C$, may provide a key regulatory mechanism in SNARE assembly. Formation of binary and ternary complexes induces additional α-helical structure in previously unstructured regions. Our data suggest a directed assembly process beginning distal to the membrane surfaces and proceeding toward them, bringing membranes into close proximity and possibly leading to membrane fusion.

The SNARE vesicle fusion machinery is present in all eukaryotes[1]. Interactions between these proteins are required for the fusion of distinct membranes. Sequence comparisons indicate extensive similarity among SNARE proteins[2,3], and a wealth of biochemical studies have highlighted conserved properties of SNARE protein interactions. A 'binary' complex is formed by members of the target membrane SNARE (t-SNARE) syntaxin and SNAP-25 families[4]. Addition of the vesicular SNARE (v-SNARE) synaptobrevin family member results in the formation of a highly stable 'ternary' complex[4–7].

Limited proteolysis has been used to identify the core folding domain of the synaptic SNARE complex of syntaxin-1A, synaptobrevin-II and SNAP-25B[8,9]. This core synaptic fusion complex is sufficient for disassembly by α-SNAP (soluble NSF attachment protein) and NSF (N-ethylmaleimide sensitive factor)[8], and it consists of the C-terminal 'H_{core}' domain from syntaxin-1A, two α-helical domains from SNAP-25B, and most of the cytoplasmic domain of synaptobrevin-II. The crystal structure of this heterotrimeric complex consists of a highly twisted four helix bundle 120 Å in length[10]. The solution NMR structure of the separate N-terminal $H_AH_BH_C$ domain of syntaxin-1A consists of a three helix bundle[11]. This domain has been implicated in the regulation of SNARE complex assembly[12].

Circular dichroism (CD) and fluorescence studies of neuronal[13,14] and yeast[15] SNAREs revealed several conserved gross structural and biophysical properties, most notably binding-induced structure formation. The above-mentioned structures represent the final assembly state of the SNAREs. Knowledge of intermediate assembly states, however, is crucial for a complete understanding of SNARE function. In this work, these interme-

diate assembly states have been characterized using NMR, which allowed a detailed mapping of the structural changes and folding processes associated with SNARE complex formation. Studies were carried out on the cytoplasmic domains of Sso1 (Fig. 1*a*), Snc1, and on the SNAP-25 like domain of Sec9, which are three yeast homologs of the neuronal SNAREs syntaxin, synaptobrevin, and SNAP-25, respectively.

To monitor binding-induced structural changes on a residue-by-residue basis, an experimental NMR strategy was used that is similar to the one employed by Schulman et al.[16]. First, resonances in ${}^1H$-${}^{15}N$ heteronuclear single quantum correlation (HSQC) spectra (obtained at pH 4.5) were assigned to specific amino acids of the ${}^{15}N$ labeled monomeric proteins. Then, persistence of these resonances was monitored after complex formation. These experiments were carried out at low temperatures (15 °C). Under these conditions, resonances from large (>30 kDa) structured regions are not detectable due to excessive broadening caused by the slow tumbling of the molecule. Thus, disappearance or severe broadening of a resonance could be explained by the corresponding residue's participation in formation of a stable, slowly tumbling large structure. It could also be explained by the residue's involvement in conformational fluctuations on a slow time scale. This latter possibility cannot be formally eliminated, but we believe it is ruled out by knowledge of homologous structures of the core synaptic fusion complex[10] and of the $H_AH_BH_C$ domain[11] of syntaxin-1A, and by CD studies of the yeast proteins (ref. 15 and data not shown). Thus, the disappearance of a resonance can be associated with formation of predominantly α-helical structure in SNARE complexes.

Sso1 is partially unstructured and Snc1 is unstructured

${}^1H$-${}^{15}N$-HSQC spectra were used to characterize the uncomplexed states of the ${}^{15}N$ labeled cytoplasmic domains of Sso1 and Snc1 (Fig. 1*a,b* respectively). Resonances were assigned to the 35 N- and 36 C-terminal residues of Sso1, and to the entire backbone of Snc1. Representative ${}^1H$-${}^{15}N$ NOESY-HSQC strips of Sso1 used for the assignments are shown in Fig. 1*d*. These resonances exhibit small amide chemical shift dispersion, clustering of glycine, serine and threonine resonances at ${}^{15}N$ chemical shifts below 115 p.p.m., and clustering of alanine ${}^{15}N$ signals at high chemical shifts around 123 p.p.m.[17,18]. Thus, Sso1 has unstructured regions at its N- and C-termini, and the entire backbone of Snc1 is unstructured. These regions likely undergo random and fast conformational sampling of the backbone, which is consistent with observed chemical shifts, coupling constants, nuclear Overhauser effect (NOE) data, and relaxation data (not shown). Peaks for the structured region of Sso1, residues 31–226, were not detectable at 15 °C. They became visible at 30 °C due to faster overall tumbling of the molecule at higher temperatures (data not shown). Our results are consistent with previously reported CD spectra[15].

The closed conformation of monomeric Sso1

The structure of the $H_AH_BH_C$ domain (Fig. 1*a*) of syntaxin-1A (ref. 11) and that of syntaxin-3 (unpublished data) consists of a three helix bundle with a large groove. The sequence of this three helix bundle maps onto residues 31–144 of Sso1 (not shown). Therefore, a structured region of at least 110 residues should be present in uncomplexed Sso1. However, our data indicate that a much larger number of resonances (195) are either absent or strongly attenuated. This suggests that the $H_AH_BH_C$ domain, a linker, and half of the H_{core} domain are

letters

structured in the uncomplexed protein (Fig. 1a). We hypothesize that a four helix bundle is formed by binding of the N-terminal half of H_{core} to the large groove presented by the $H_A H_B H_C$ domain.

Surface plasmon resonance binding experiments using syntaxin-1A constructs showed that the H_{core} domain binds weakly to an N-terminal domain which includes the $H_A H_B H_C$ domain[6]. Our data indicate that the $H_A H_B H_C$ domain of Sso1 specifically binds to the N-terminal half of H_{core} (Fig. 2a–d). First, the isolated $H_A H_B H_C$ domain co-migrates with the isolated

H_{core} domain during size exclusion chromatography, providing evidence for the direct interaction of these two regions of the protein (Fig. 2a). Comparison of CD thermal melting curves indicates that the $H_A H_B H_C$ domain is dramatically stabilized by the N-terminal half of the H_{core} domain (Fig. 2b). In fact, the 196-residue fragment has nearly the same melting temperature as the full length protein. The molar ellipticities of the Sso1 fragments together with calculated estimates of the number of α-helical residues are shown in Fig. 2c. The fragment containing the N-terminal half of H_{core} has ~50 additional residues in an α-helical conformation when compared to spectra of fragments that do not contain this portion of the H_{core} domain. Finally, the ^1H-^{15}N-HSQC spectrum of the ^{15}N labeled H_{core} domain, Sso1(193–265), (Fig. 2d, black) displays significant peak shifts when unlabeled $H_A H_B H_C$ is added (Fig. 2d, red). All these results confirm that the $H_A H_B H_C$ three helix bundle interacts with the N-terminal half of the H_{core} domain. Thus, the $H_A H_B H_C$ domain and the H_{core} domain most likely form a four helix bundle (Fig. 5b).
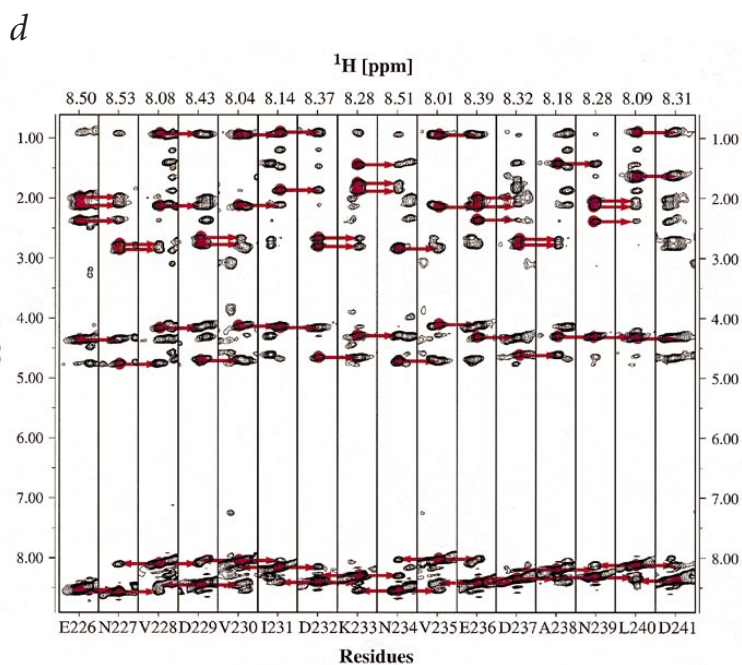
Binding induced structure in the Sso1–Sec9 complex

CD measurements indicated significant induction of α-helicity upon binary complex formation of Sso1 and Sec9[15]. HSQC NMR spectroscopy identified specific residues of Sso1 that participate in this conformational transition (Fig. 3a, red peaks). Cross peaks are strongly attenuated or absent for residues Asn 227–Val 235 (Fig. 3b, filled histogram). Presumably, these previously unstructured residues are involved in interactions that result in
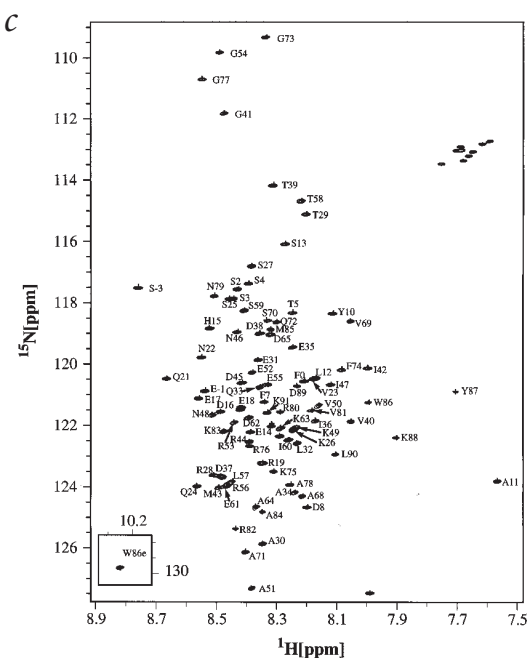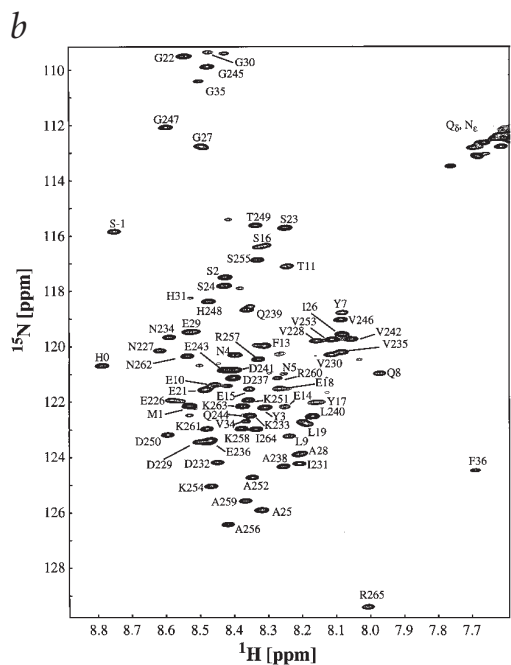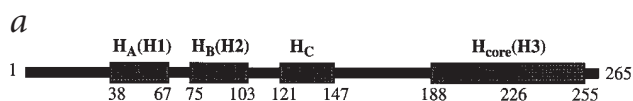
Fig. 1 Structural characterization of the cytoplasmic domains of uncomplexed Sso1 and Snc1. Spectra were collected with the proteins in 20 mM sodium acetate, pH 4.5 and 200 mM NaCl in H_2O:^2H_2O (9:1). **a**, Domain structure of Sso1. **b**, ^1H-^{15}N-HSQC spectrum of uncomplexed Sso1. Assigned resonances correspond to unstructured regions at the N- and C-terminus. **c**, ^1H-^{15}N-HSQC spectrum of uncomplexed Snc1. Assigned resonances correspond to the entire cytoplasmic domain of the protein. **d**, Representative ^1H-^{15}N-NOE-HSQC strips from which assignments for Sso1 were derived.
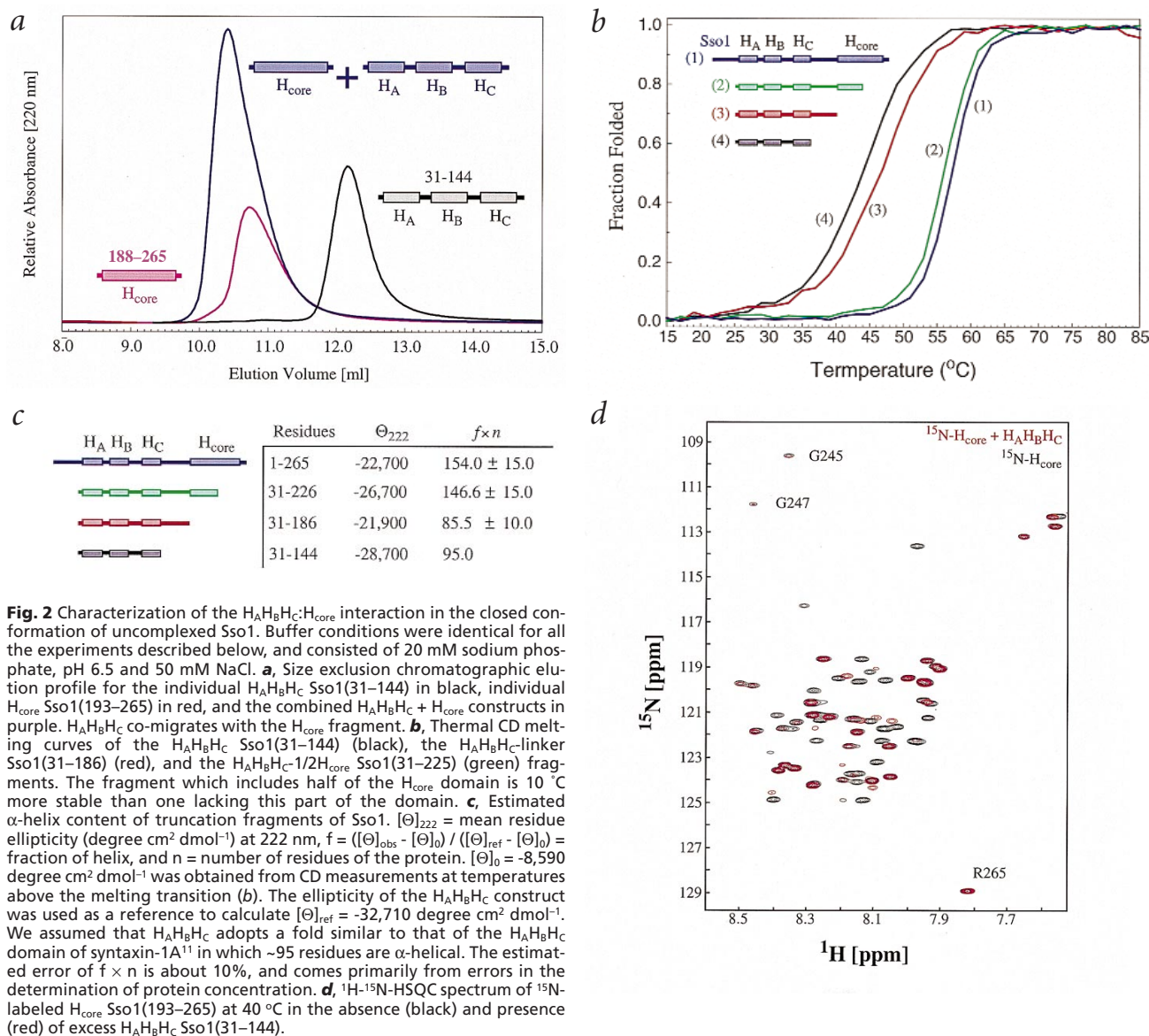
letters

Fig. 2 Characterization of the $H_A H_B H_C$:H_{core} interaction in the closed conformation of uncomplexed Sso1. Buffer conditions were identical for all the experiments described below, and consisted of 20 mM sodium phosphate, pH 6.5 and 50 mM NaCl. **a**, Size exclusion chromatographic elution profile for the individual $H_A H_B H_C$ Sso1(31–144) in black, individual H_{core} Sso1(193–265) in red, and the combined $H_A H_B H_C$ + H_{core} constructs in purple. $H_A H_B H_C$ co-migrates with the H_{core} fragment. **b**, Thermal CD melting curves of the $H_A H_B H_C$ Sso1(31–144) (black), the $H_A H_B H_C$-linker Sso1(31–186) (red), and the $H_A H_B H_C$-1/2H_{core} Sso1(31–225) (green) fragments. The fragment which includes half of the H_{core} domain is 10 °C more stable than one lacking this part of the domain. **c**, Estimated α-helix content of truncation fragments of Sso1. $[\Theta]_{222}$ = mean residue ellipticity (degree cm^2 dmol^{-1}) at 222 nm, f = $([\Theta]_{obs} - [\Theta]_0) / ([\Theta]_{ref} - [\Theta]_0)$ = fraction of helix, and n = number of residues of the protein. $[\Theta]_0$ = -8,590 degree cm^2 dmol^{-1} was obtained from CD measurements at temperatures above the melting transition (**b**). The ellipticity of the $H_A H_B H_C$ construct was used as a reference to calculate $[\Theta]_{ref}$ = -32,710 degree cm^2 dmol^{-1}. We assumed that $H_A H_B H_C$ adopts a fold similar to that of the $H_A H_B H_C$ domain of syntaxin-1A[11] in which ~95 residues are α-helical. The estimated error of f × n is about 10%, and comes primarily from errors in the determination of protein concentration. **d**, ^{1}H-^{15}N-HSQC spectrum of ^{15}N-labeled H_{core} Sso1(193–265) at 40 °C in the absence (black) and presence (red) of excess $H_A H_B H_C$ Sso1(31–144).

formation of structure. In the binary complex, 24 C-terminal residues of Sso1 remain unstructured. A model of the binary complex can be derived from these results, from CD studies[15], and from the crystal structure of the core synaptic fusion complex[10]. The binary complex likely consists of the $H_A H_B H_C$ three helix bundle and an additional three helix bundle to which Sec9 contributes two core complex α-helices and Sso1 provides the H_{core} domain (Fig. 5b). In this complex, the H_{core} domain is no longer bound to the $H_A H_B H_C$ domain, and Sso1 adopts an 'open' conformation.

Additional induced structure in the Sso1–Sec9–Snc1 complex

Additional structural transitions occur in Sso1 and Snc1 upon formation of the ternary complex of Sso1, Sec9 and Snc1 (filled histogram in Fig. 4a,b). The entire C-terminal region of the cytoplasmic domain of Sso1 (Fig. 5) becomes structured. About two thirds of the cytoplasmic domain of Snc1 also

become structured (Fig. 5). This agrees well with the X-ray crystal structure of the core synaptic fusion complex[10]. Several new cross-peaks appear in ^{1}H-^{15}N-HSQC spectra of the ternary complex (not shown). These new resonances could reflect changes in the chemical shifts of unstructured residues. N-terminal cross peaks in the ^{1}H-^{15}N-HSQC spectrum of Sso1 do not undergo significant detectable changes (Fig. 4a). Thus, binding of Snc1 to the binary complex only affects the C-terminus of Sso1, suggesting that its N-terminal $H_A H_B H_C$ domain is conformationally independent from the core fusion complex (Fig. 6d). Electron microscopic images of the entire synaptic fusion complex[19] also support the idea that the N-terminal domain is peripheral to the complex, connected only by a flexible linker.

Model of SNARE complex assembly

A summary of the observed structural data is shown in Fig. 5a.
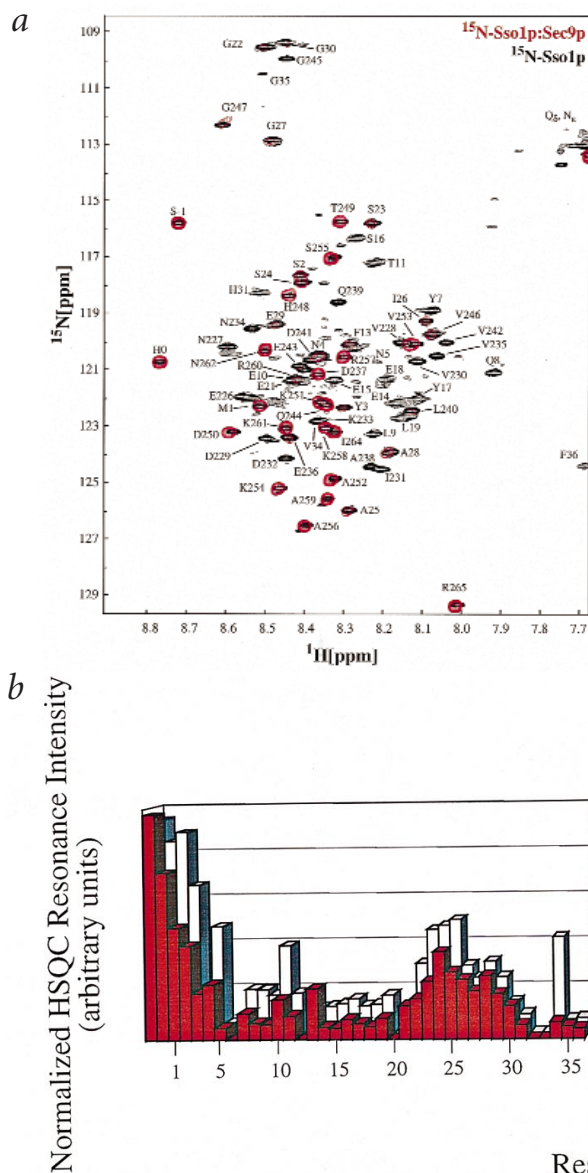
letters

Fig. 3 Unstructured regions and binding induced structure formation in the binary complex of Sso1 and Sec9. Samples were prepared as in Fig. 1. **a**, ¹H-¹⁵N-HSQC spectra of uncomplexed ¹⁵N-Sso1 are shown in black. Overlaid, in red, are resonances from ¹⁵N-Sso1 in the binary Sso1–Sec9 complex. Line widths along the ¹⁵N dimension are broader in the binary complex spectrum due to differences in data acquisition (see Methods). **b**, The same data are also shown in histogram format for the assigned N- and C-terminal residues. Peak heights were obtained for each residue, normalized by the intensity of a peak that is unstructured in both spectra (in this case Arg 265), and then plotted as a function of residue number. Spectral intensities for uncomplexed Sso1 are shown as open bars, and intensities corresponding to Sso1 bound to Sec9 are shown as red bars. Unresolved resonance intensities and resonance intensities corresponding to unassigned residues or prolines were set to zero. The sequence numbering begins at -1 in order to account for extra residues which result from the bacterial expression vector used.

These data suggest a possible model for SNARE assembly events (Fig. 5*b*). Uncomplexed Snc1 (Fig. 1*c*) and uncomplexed Sec9 are entirely unstructured[15], as are N- and C-terminal segments of monomeric Sso1 (Fig. 1*b*). These studies have been performed using truncated recombinant Sso1 and Snc1 lacking transmembrane domains. While it is likely that the presence of the transmembrane domains and the proximity of the membrane itself affect the conformation of the proteins, these unstructured regions may be intrinsically flexible *in vivo*. For example, in the neuronal case, flexibility of uncomplexed synaptobrevin and of uncomplexed syntaxin may explain their susceptibility to cleavage by neurotoxins. We suggest that binding-induced structure formation is a fundamental feature of SNARE function.

Our data for Sso1 demonstrate that the uncomplexed protein folds back onto itself, probably forming a four helix bundle comprised of three α-helices from the $H_AH_BH_C$ domain and a fourth

α-helix provided by an N-terminal portion of the H_{core} domain (Fig. 5*b* step (i)). This 'closed' state may be akin to the proposed syntaxin* state[20], and is likely to represent a non-fusogenic conformation of the protein[12]. Conformational switching of the H_{core} domain is likely to be a crucial mechanism for regulating SNARE assembly[12]. Soluble factors that stabilize the $H_AH_BH_C$:H_{core} interaction may inhibit SNARE complex assembly. For example, Sec1 may function in this capacity[21–24]. Furthermore, SNARE complex assembly may be promoted by proteins that displace the H_{core} domain from the three helix bundle $H_AH_BH_C$ domain. Once H_{core} is displaced, the $H_AH_BH_C$ domain may play a role in the recruitment of accessory proteins[11].

Formation of the binary complex between Sso1 and Sec9 constitutes an intermediate step in SNARE complex assembly. Sso1 switches to an open conformation, with the H_{core} domain binding to Sec9 instead of to the $H_AH_BH_C$ domain. This highlights the importance of the N-terminal portion of H_{core} as a target for reg-
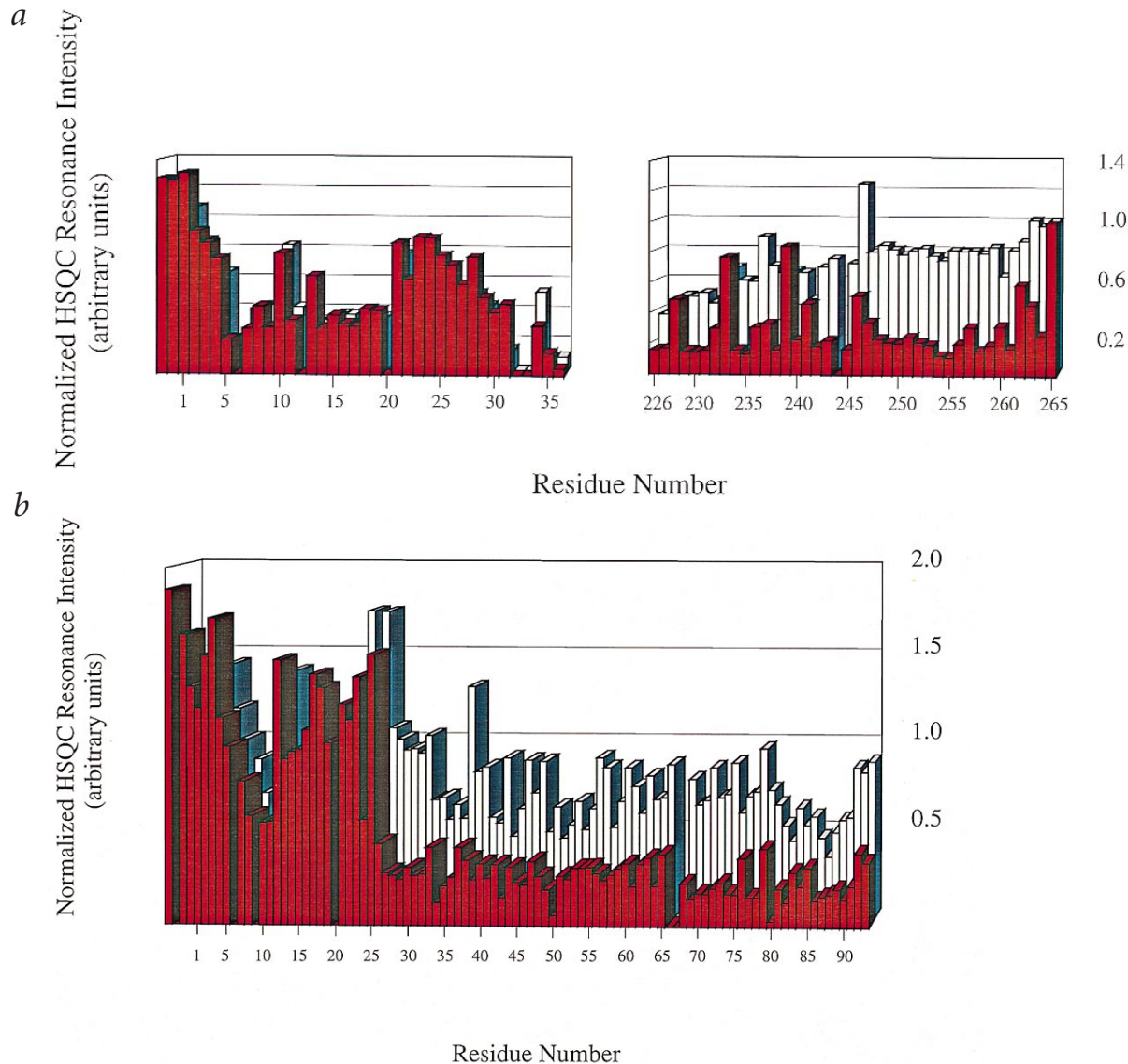
a

b

Fig. 4 Additional induced structure upon formation of the ternary complex of Sso1, Sec9 and Snc1. Peak intensities of HSQC spectra are shown as histograms. Buffer concentrations for these spectra were as for Figs 1 and 3 with the addition of 2 M urea, which was required to solubilize the ternary complex. *a*, Sso1: open bars indicate spectral intensities for uncomplexed ^{15}N labeled Sso1, and red bars correspond to HSQC intensities of ^{15}N labeled Sso1 in the ternary complex. Intensities were normalized using the intensity of Arg 265 as described in Fig. 3. *b*, Snc1: Open bars indicate normalized spectral intensities from uncomplexed ^{15}N labeled Snc1, and red bars indicate spectral intensities from ^{15}N labeled Snc1 bound to Sso1 and Sec9. In this case the intensity of Ser 5 was used for normalization. The sequence numbering begins at -3 in order to account for extra residues which result from the bacterial expression vector used.

ulation and recognition. In this complex, a C-terminal portion (24 residues) of the H$_{core}$ domain remains unstructured. These residues may function as a flexible tether to allow the Sso1–Sec9 template more freedom to adopt an orientation favorable for binding to Snc1. Thus, we modeled the binary complex as a three helix bundle (Fig. 5*b*, stage (ii)) which is significantly shorter than the fully assembled core synaptic fusion complex[10]. This model is based on the structure of the synaptic fusion complex[10] and is inferred from the *in vitro* 1:1 stoichiometry of the yeast binary complex[15].

For the final assembly stage (iii) of the ternary complex, we propose a hypothetical transient intermediate in which a part

of Snc1 binds to the three helix template presented by the H$_{core}$ domain of Sso1 bound to Sec9 (Fig. 5*b*). The flexible residues tethering the binary complex to the membrane make it probable that Snc1 binding begins distant from the membrane surface and proceeds toward it. This assembly process may bring vesicular and target membranes into close proximity (Fig. 5*b*, stage (iv)), or may induce sufficient strain[10], leading to membrane fusion.

Methods
NMR sample preparation of yeast SNAREs. The cytoplasmic domains of Sso1 and Snc1, the SNAP-25-like domain of Sec9, the

letters

Fig. 5 *a*, Summary of the NMR data mapping unstructured or flexible regions in the cytoplasmic domains of uncomplexed Sso1 and Snc1, and when in the binary or ternary complex. Red shaded regions are unstructured according to the NMR data. α-helical regions are indicated by boxes and are based on the structure of the core synaptic fusion complex[10] and on the structure of the $H_A H_B H_C$ domain from syntaxin-3 (unpublished data). *b*, Hypothetical model of SNARE protein assembly events. (i) The $H_A H_B H_C$ domain of monomeric Sso1, in orange, binds the N-terminal half of its H_{core} domain (shown in red) to form a four helix bundle. (ii) The binary complex of Sso1 and Sec9. (iii) Sec9 and the H_{core} domain of Sso1 form a partially assembled three helix bundle scaffold that facilitates binding to Snc1. (iv) Ternary complex before membrane fusion.
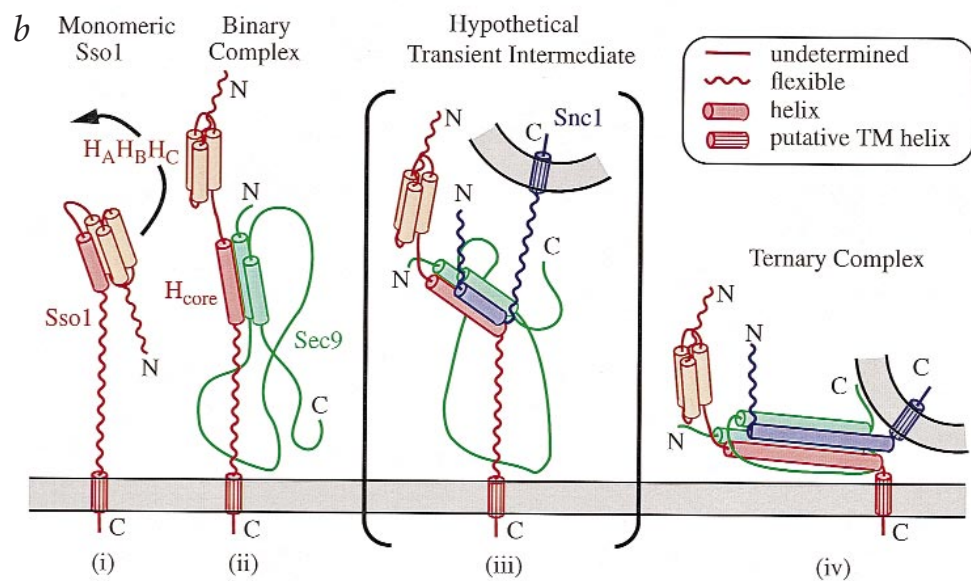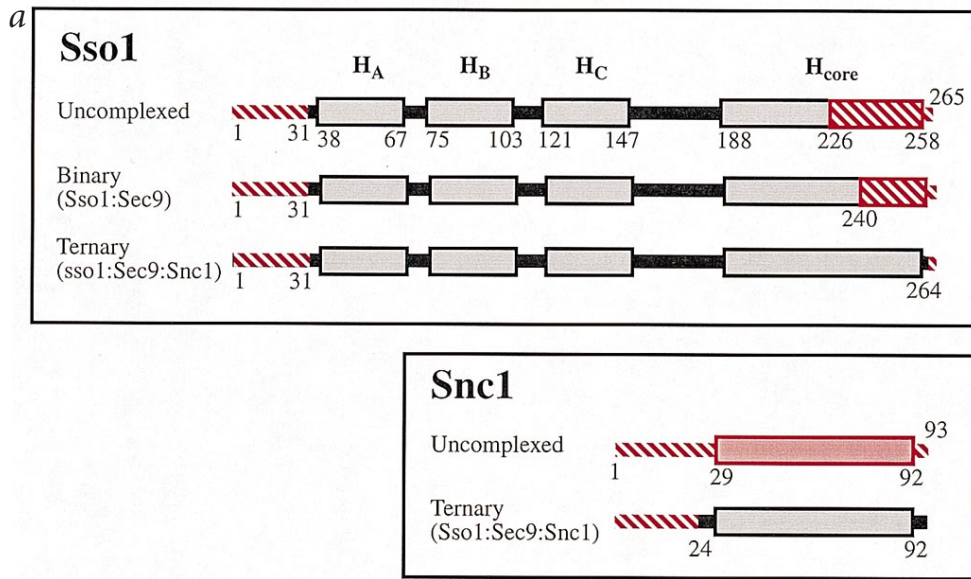
binary and ternary complexes were purified following published procedures[15]. Purification of the Sso1 deletion fragments was similar to that of the full length protein. Uniformly ^{15}N labeled Sso1, Sso1(193–265), and Snc1 were isolated from bacteria grown in M9 minimal media supplemented with 35 mg l^{-1} thiamine, 10 mM MgCl$_2$, 0.8% glucose, and 0.1% ^{15}NH$_4$Cl. Protein induction was carried out at 25 °C for 5 h. NMR samples of uncomplexed and complexed ^{15}N labeled Snc1 and Sso1 contained 20 mM sodium acetate, pH 4.5, and 200 mM NaCl in H$_2$O/^{2}H$_2$O (9:1). Low pH was required to reduce amide hydrogen exchange with solvent. 2 M urea was required to facilitate solubility of the ternary complex of Sso1, Sec9 and Snc1. CD signatures of both Sso1 and the ternary complex with and without urea and over a broad pH range were comparable, while thermal denaturation monitored by CD at 222 nm indicated a small (5 °C) drop in thermal stability upon addition of 2 M urea (data not shown). ^{1}H-^{15}N-HSQC spectra of the Sso1(193–265) fragment were recorded in 20 mM sodium phosphate, pH 6.5, and 50 mM NaCl at 0.3 mM protein concentration. Protein concentrations of the NMR samples of uncomplexed Sso1 and Snc1 were 1.0–1.5 mM. The concentration of the binary and ternary complex samples was 0.05 mM.

NMR data collection and analysis for yeast SNARE proteins. Gradient enhanced ^{1}H-^{15}N-HSQC[25] spectra for uncomplexed Sso1 and Snc1 were collected with 128 complex t_1 increments of 1K complex data points and 32 transients per FID at 0 M and 2 M urea. Similar spectra were collected for complexed Sso1 and Snc1 with 32 complex t_1 increments of 1K complex data points and 128 transients per FID. Spectral sweep widths were 24.7 and 16.0 p.p.m. for the ^{15}N (F$_1$) and ^{1}H (F$_2$) dimensions, respectively. NMR data were recorded on Varian 600 MHz Unity+ and 800 MHz Inova instruments. Spectra of the full-length proteins and their complexes were acquired at 15 °C. Spectra of the Sso1(193–265) fragment were acquired at 40 °C.

^{1}H signals of all spectra were referenced to internal 3-(trimethylsilyl)propionate-2,2,3,4-d$_4$ (Cambridge Isotope Laboratories). ^{15}N was referenced indirectly to ^{1}H (ref. 26). ^{1}H and ^{15}N resonances of uncomplexed Sso1 and Snc1 were assigned by standard sequential assignment procedures[27,28] using the program XEasy[29] applied to ^{15}N-edited 3D gradient-enhanced NOESY-HSQC and TOCSY-HSQC[30] spectra collected with mixing times of 120 ms and 67 ms, respectively. Sequential and side chain ^{1}H assignment were facilitated by long (>6) stretches of unambiguous sequential NOE connectivities and by

letters

clustering of Gly, Ser, Thr and Ala resonances in the ^{1}H-^{15}N-HSQC spectra typical of chemically denatured proteins[17,18]. All NMR data were processed using Felix95 (Biosym).

CD spectroscopy. The cytoplasmic domain of Sso1 and truncation constructs were dialyzed against 20 mM sodium phosphate buffer, pH 6.5, containing 50 mM NaCl. Protein concentrations were determined by internally standardized amino acid analysis following acid hydrolysis (performed by the W.M. Keck Foundation Biotechnology Resource Laboratory at Yale University). Far UV CD spectra were recorded on an AVIV model 62DS CD spectrometer at 15 °C in a 0.1 mm Hellma quartz cuvette between 280 nm to 200 nm. Five scans were averaged with a signal averaging time of 1 s and a step size of 1 nm. Thermal denaturation was performed in the same cuvette, with measurements taken every 2 °C between 15 and 85 °C with 2 min equilibration and 5 s signal averaging at each temperature.

Assignments. Assignments have been deposited in the BioMagResBank (BMRB) database (accession numbers 4286 and 4287 for Snc1 and Sso1, respectively).

1. Ferro-Novick, S. and Jahn, R. *Nature* **370**, 191–193 (1994).
2. Weimbs, T. *et al. Proc. Nat. Acad. Sci. USA* **94**, 3046–3051 (1997).
3. Terrian, D.M. & White, M.K. *Eur. J. Cell. Biol*. **73**, 198–204 (1997).
4. Rossi, G., Salminen, A., Rice, L.M., Brunger, A.T. & Brennwald, P. *J. Biol. Chem*. **272**, 16610-16617 (1997).
5. Bennett, M.K. *Curr. Opin. Cell. Biol*. **7**, 581-586 (1995).
6. Calakos, N., Bennett, M.K., Peterson, K.E. & Scheller, R.H. *Science* **263**, 1146–1149 (1994).
7. Lin, R.C. & Scheller, R.H. *Neuron* **19**, 1087–1094 (1997).
8. Fasshauer, D., Eliason, W.K., Brunger, A.T. & Jahn, R. *Biochemistry* **37**, 10354–10362 (1998).
9. Poirier, M.A. *et al. J. Biol. Chem*. **273**, 11370–11377 (1998).
10. Sutton, R.B., Fasshauer, D., Jahn, R. & Brunger, A.T. *Nature* **395**, 347-353 (1998).
11. Fernande, I. *et al. Cell* **94**, 841–849 (1998).
12. Nicholson, K. L. *et al. Nature Struct. Biol*. **5**, 793–802 (1998).
13. Fasshauer, D., Otto, H., Eliason, W.K., Jahn, R. & Brunger, A.T. *J. Biol. Chem*. **272**, 28036–28041 (1997).
14. Fasshauer, D., Bruns, D., Shen, B., Jahn, R. & Brunger, A.T. *J. Biol. Chem*. **272**, 4582–4590 (1997).
15. Rice, L.M., Brennwald, P. & Brunger, A.T. *FEBS Lett*. **415**, 49–55 (1997).
16. Schulman, B.A., Kim, P.S., Dobson, C.M. & Redfield, C. *Nature Struct. Biol*. **4**, 630–634 (1997).
17. Schwalbe, H. *et al. Biochemistry* **36**, 8977–91 (1997).
18. Wishart, D.S., Bigam, C.G., Holm, A., Hodges, R.S. & Sykes, B.D. *J. Biomol. NMR* **5**, 67–81 (1995).
19. Hanson, P.I., Roth, R., Morisaki, H., Jahn, R. & Heuser, J.E. *Cell* **90**, 523–535 (1997).
20. Hanson, P.I., Otto, H., Barton, N. & Jahn, R. *J. Biol. Chem*. **270**, 16955–16961 (1995).
21. Aalto, M.K., Ronne, H. & Keranen, S. *EMBO J*. **12**, 4095–4104 (1993).
22. Hata, Y., Slaughter, C.A. & Südhof, T.C. *Nature* **366**, 347–351 (1993).
23. Garcia, E.P., McPherson, P.S., Chilcote, T.J., Takei, K. & De Camilli, P. *J. Cell. Biol*. **129**, 105–120 (1995).
24. Pevsner, J., Hsu, S.C. & Scheller, R.H. *Proc. Natl. Acad. Sci. USA* **91**, 1445–9 (1994).
25. Kay, L.E., Keifer, P. & Saarinen, T. *J. Am. Chem. Soc*. **114**, 10663–10665 (1992).
26. Live, D.H., Davis, D.G., Agosta, W.C. & Cowburn, D. *J. Am. Chem. Soc*. **106**, 1939–1943 (1986).
27. Marion, D. *et al. Biochemistry* **28**, 6150–6156 (1989).
28. Driscoll, P.C., Clore, G.M., Marion, D., Wingfield, P.T. & Gronenborn, A.M. *Biochemistry* **29**, 3542–3556 (1990).
29. Bartels, C., Xia, T.H., Billeter, M., Guntert, P. & Wüthrich, K. *J. Biomol. NMR* **6**, 1–10 (1995).
30. Zhang, O., Kay, L.E., Olivier, J.P. & Forman-Kay, J.D. *J. Biomol. NMR* **4**, 845–858 (1994).

Structural basis for HLA-DQ binding by the streptococcal superantigen SSA

Eric Sundberg and Theodore S. Jardetzky

Department of Biochemistry, Molecular Biology and Cell Biology, Northwestern University, Evanston Illinois 60208, USA.

Streptococcal superantigen (SSA) is a 28,000 M_r toxin originally isolated from a pathogenic strain of *Streptococcus pyogenes* that has 60% sequence identity with staphylococcal enterotoxin B (SEB). SSA and SEB, however, do not compete for binding on the surfaces of cells expressing MHC class II molecules. This behavior had been ascribed to SSA and SEB binding to distinct sites on, or different subsets of, HLA-DR molecules. Here we demonstrate that SSA binds predominantly to HLA-DQ, rather than to HLA-DR molecules, and present the crystal structure of SSA at 1.85 Å resolution. These data provide a structural basis for interpreting the interaction of SSA with HLA-DQ molecules as well as a foundation for understanding bacterial superantigen affinities for distinct MHC isotypes.

Bacterial superantigens (bSAgs) bind as folded proteins to both major histocompatibility complex (MHC) class II molecules on the surfaces of antigen-presenting cells and T cell receptor Vβ domains on T cells[1,2]. The resulting activation of T cells correlates with a number of human diseases, including food poisoning and toxic shock syndrome, and may play an important role in autoimmune diseases[2–4]. Although bSAgs share highly homologous sequences, as well as similar three-dimensional folds, binding to MHC class II molecules depends on the biochemical and structural states of class II molecules expressed on the cell surface. Understanding the molecular basis for bSAg–MHC affinities and specificities may provide fundamental insights into MHC function as well as the role of superantigens in disease.

The cocrystal structures of SEB[5] and toxic shock syndrome toxin-1[6] (TSST-1), complexed with the class II molecule HLA-DR1, show that these two superantigens have overlapping MHC binding sites, although functional studies show that they do not compete for MHC class II binding on all DR1 molecules. Although bSAgs bind outside of the conventional MHC–peptide binding site, the affinity of the bSAg–MHC interaction is affected by peptides bound to the MHC molecule[7]. This was first demonstrated for the bSAgs staphylococcal enterotoxin A (SEA) and TSST-1, which may both interact directly with MHC-bound peptides[8]. More recently, binding studies using cell lines expressing various components of the antigen-processing machinery (invariant chain [Ii] and HLA-DM) have shown that the interaction of SEB, SEA and TSST-1 to HLA-DR is dependent on the particular processing machinery of the MHC-expressing cell line and, subsequently, what is displayed in the class II binding groove on the cell surface[9].